Decentralized Time and Energy-Optimal Control of Connected and Automated Vehicles in a Roundabout with Safety and Comfort Guarantees

Kaiyuan Xu, Christos G. Cassandras, *Life Fellow, IEEE,* Wei Xiao, *Member, IEEE*

***Abstract*—We consider the problem of controlling Connected and Automated Vehicles (CAVs) traveling through a roundabout so as to jointly minimize their travel time, energy consumption, and centrifugal discomfort while providing speed-dependent and lateral roll-over safety guarantees, as well as satisfying velocity and acceleration constraints. We first develop a systematic approach to determine the safety constraints for each CAV dynamically, as it moves through different merging points in the roundabout. We then derive the unconstrained optimal control solution which is subsequently optimally tracked by a real-time controller while guaranteeing that all constraints are always satisfied. Simulation experiments are performed to compare the controller we develop to a baseline of human-driven vehicles, showing its effectiveness under symmetric and asymmetric roundabout configurations, balanced and imbalanced traffic rates, and different sequencing rules for CAVs.**

I. Introduction

The performance of traffic networks critically depends on the control of conflict areas such as intersections, roundabouts and merging roadways which define the main bottlenecks in these networks [1]. Coordinating and controlling vehicles in these conflict areas is a challenging problem in terms of ensuring safety and passenger comfort while minimizing congestion and energy consumption [2], [3]. The emergence of Connected and Automated Vehicles (CAVs) provides a promising solution to this problem through better information utilization and more precise trajectory design. The automated control of vehicles has gained increasing attention with the development of new traffic infrastructure technologies [4], [1].

Both centralized and decentralized methods have been studied to deal with the control and coordination of CAVs at conflict areas. Centralized mechanisms are often used in forming platoons in merging problems [5] and determining passing sequences at intersections [6]. These approaches tend to work better when the safety constraints are independent of speed and they generally require significant computation resources, especially when traffic is heavy. They are also not easily amenable to disturbances.

Decentralized mechanisms restrict all computation to be done on board each CAV with information sharing limited to a small number of neighbor vehicles [7]–[10]. Optimal control problem formulations are often used, with Model Predictive Control (MPC) techniques employed as an alternative to account for additional constraints and to compensate for disturbances by re-evaluating optimal actions [11]–[13]. The objectives in such problem formulations typically target the minimization of acceleration or the maximization of passenger comfort (measured as the acceleration derivative or jerk). An alternative to MPC has recently been proposed through the use of Control Barrier Functions (CBFs) [14], [15] which provide provable guarantees that safety constraints are always satisfied under very general nonlinear vehicle dynamics affine in control.

In this paper, we build on the use of optimal control and CBF-based methods as applied to unsignalized intersections [16] and merging [17] to study roundabouts with all traffic consisting of CAVs. There are several similarities between merging, intersections, and roundabouts. The single-lane merging problem [17] contains a single Merging Point (MP) where safety constraints must be guaranteed, while CAVs follow the same moving direction in each lane. In intersection problems, CAVs have a number of possible paths which conflict at multiple MPs restricted to a small area. On the other hand, in a roundabout, CAVs have the same moving direction (either clockwise or counterclockwise), but multiple possible paths which cross at multiple MPs. A roundabout problem can be dealt with as either a whole system, like an intersection, or it can be decomposed into several coupled merging problems.

Roundabouts are important components of a traffic network because they usually perform better than typical intersections in terms of efficiency and safety [18]. However, they can become significant bottleneck points as the traffic rate increases due to an inappropriate priority system, resulting in significant delays when the circulating flow is heavy. Previous studies mainly focus on conventional (human-driven) vehicles and try to solve the problem through improved road design or traffic signal control [19]–[21]. More recently, however, researchers have proposed methods for decentralized optimal control of CAVs in a roundabout based on formulating an optimal control problem with an analytical solution provided in [22]. The problem is decomposed so that first the minimum travel time problem is solved under the assumption that all vehicles use the same maximum speed within the roundabout. Then, fixing this time, the control input that minimizes the energy consumption is derived analytically. The general framework for decentralized optimal control of CAVs used in intersections

This work was supported in part by NSF under grants ECCS-1931600, DMS-1664644 and CNS-1645681, by ARPAE under grant DE-AR0001282, by AFOSR under grant FA9550-19-1-0158, and by the MathWorks.

K. Xu and C. G. Cassandras are with the Division of Systems Engineering and Center for Information and Systems Engineering, Boston University, Brookline, MA, 02446, USA {xky, cgc}@bu.edu

W. Xiao is with the Computer Science and Artificial Intelligence Lab, Massachusetts Institute of Technology. weixy@mit.edu

is implemented for roundabouts in [23]. The analysis is similar to [22] except that there is no circulating speed assumption.

In this paper, we formulate an optimal control problem for controlling CAVs traveling through a roundabout. The main contributions are as follows. First, unlike [22], [23], we *jointly* minimize the travel time and energy consumption while also considering speed-dependent safety constraints at a set of MPs rather than merging zones, which makes solutions less conservative by improving roadway utilization. Second, unlike our earlier work [24] where we considered roundabouts consisting of only straight road segments, we analyze circular roundabout configurations where we include comfort constraints guaranteed to be satisfied. Third, we overcome the computational complexity of solving such an optimal control problem analytically, by adopting the joint Optimal Control and Barrier Function (OCBF) approach in [15]: we first derive the optimal solution when no constraints become active and subsequently optimally track this solution while also *guaranteeing* the satisfaction of all constraints at all times through utilizing the forward invariance property of CBFs. We divide the roundabout into separate merging problems so as to introduce different resequencing rules depending on the MP. Thus, we will show that the commonly used First-In-First-Out (FIFO) sequencing policy does not perform well in many "asymmetric" configurations and explore an alternative sequencing policy, termed Shortest Distance First (SDF), which our experimental results show to be superior to FIFO.

The paper is organized as follows. In Section II, the roundabout problem is formulated as an optimal control problem that jointly minimizes travel times and energy consumption with safety and vehicle limitation constraints. In Section III, a decentralized framework is provided to determine the safety constraints related to a given CAV as it moves through different MPs in the roundabout. An OCBF controller is designed in Section IV where several CBFs are introduced to guarantee the satisfaction of all constraints. Simulation results are presented in Section V showing significant improvements in the performance of the OCBF controller compared to a baseline of human-driven vehicles. Conclusions are provided in Section VI.

II. Problem Formulation

We consider the roundabout model shown in Fig. 1 with 3 entries and 3 exits. Extending our analysis to more than 3 entry and exit points is straightforward. We assume that each road segment has a single lane (extensions to multiple lanes and MPs are possible following natural extensions we have already applied for merging [25] and for signal-free intersections [26]).

A coordinator, i.e., a Road Side Unit (RSU) associated with the roundabout, records the information associated with each CAV and maintains a queue table (see Fig. 1) with CAVs orfered as they enter the CZ. The CAVs communicate with the coordinator but are not controlled by it; rather, control inputs are evaluated on-board each CAV in a *decentralized* way. Each CAV is assigned a unique index upon arrival at the CZ which is used to determine its passing order (i.e., the order

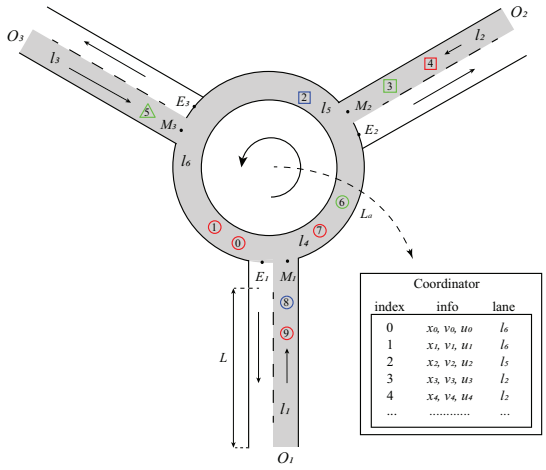

Fig. 1. CAVs randomly enter the roundabout from three different origin points O_1, O_2 and O_3 and have randomly assigned exit points E_1, E_2 and E_3. The gray road segments form the Control Zone (CZ) within which CAVs can share information and thus be automatically controlled. The entry road segments are connected with the circular part at the three Merging Points (MPs) labeled as M_1, M_2 and M_3 where CAVs from different road segments may potentially collide with each other. A circle, square and triangle represent CAVs entering from O_1, O_2 and O_3 respectively. The color red, green and blue represents exiting from E_1, E_2 and E_3 respectively.

in which CAVs go through MPs). The most common scheme for maintaining such a passing order is the First-In-First-Out (FIFO) policy based on each CAV's arrival time at the CZ. The FIFO policy is one of the simplest schemes, yet works well in many occasions as also shown in [27]. For simplicity, in what follows we use the FIFO policy to illustrate the construction of the coordinator queue table, but we point out that any passing order policy may be used, such as the Dynamic Resequencing (DR) method in [28]. We also introduce an alternative policy in Section III.

Let $S(t)$ be the set of CAV indices in the coordinator queue table at time t whose cardinality is $N(t)$. When a new CAV arrives, it is allocated the index $N(t)+1$. Each time a CAV i leaves the CZ, it is dropped and all CAV indices larger than i decrease by one. When CAV $i \in S(t)$ is traveling in the roundabout, there are several important *events* whose times are used in our analysis: (i) CAV i enters the CZ at tme t_i^0, (ii) CAV i arrives at MP M_k at time t_i^k, $k \in \{1,2,3\}$, (iii) CAV i leaves the CZ at time t_i^f. Based on this setting, we can formulate an optimal control problem as described next.

Vehicle Dynamics Denote the distance from the origin $O_j, j \in \{1,2,3\}$ to the current location of CAV i along its trajectory as $x_i^j(t)$. However, since the CAV's unique identity i contains the information about the CAV's origin O_j, we can use $x_i(t)$ instead of $x_i^j(t)$ (without any loss of information) to describe the vehicle dynamics as

$$\begin{bmatrix} \dot{x}_i(t) \\ \dot{v}_i(t) \end{bmatrix} = \begin{bmatrix} v_i(t) \\ u_i(t) \end{bmatrix} \tag{1}$$

where v_i is the velocity of CAV i along its trajectory and u_i is the acceleration (control input). In this paper, we focus on planning optimal trajectories that guarantee safety while ignoring lateral vehicle motion. The lateral vehicle offset can also be dealt with by using detailed models (e.g., the 7-state

model in [29]) and auxiliary methods like MPC following the same framework as in this paper.

Objective 1 Minimizing the travel time $J_{i,1} = t_i^f - t_i^0$ where t_i^0 and t_i^f are the times CAV i enters and exits the CZ respectively.

Objective 2 Minimizing energy consumption:

$$J_{i,2} = \int_{t_i^0}^{t_i^f} C_i(u_i(t))dt \tag{2}$$

where $C_i(\cdot)$ is a strictly increasing function of its argument. Since the energy consumption rate is a monotonic function of the acceleration, we adopt this general form to achieve energy efficiency.

Objective 3 Maximizing centrifugal comfort:

$$J_{i,3} = \int_{t_i^0}^{t_i^f} \kappa(x_i(t))v_i^2(t)dt \tag{3}$$

where $\kappa(x_i)$ is the curvature of the road at position x_i. As the aim is to minimize the centrifugal force of the vehicle, the curvature $\kappa(x_i)$ has the form of $\frac{1}{r(x_i)}$, where $r(x_i)$ is the radius of the road at position x_i.

Constraint 1 (Rear-end safety constraint) Let i_p denote the index of the CAV which immediately precedes CAV i on the same road segment as i, if one exists. The distance between i_p and i, defined as $z_{i,i_p}(t) \equiv x_{i_p}(t) - x_i(t)$, should satisfy a speed-dependent constraint:

$$z_{i,i_p}(t) \geq \varphi v_i(t) + \delta, \quad \forall t \in [t_i^0, t_i^f], \quad \forall i \in S(t) \tag{4}$$

where φ denotes the reaction time (as a rule, $\varphi = 1.8s$ is suggested, see [30]), and δ denotes the minimum safe distance between CAVs (in general, we may use δ_i to make this distance CAV-dependent but will use a fixed δ for simplicity). Note that the preceding CAV index i_p may change after road segment changing events and is updated by the method described in section III-B.

Constraint 2 (Safe merging constraint) Let $t_i^k, k \in \{1, 2, 3\}$ be the arrival time of CAV i at MP M_k. Let i_m denote the index of the CAV that CAV i may collide with when arriving at its next MP M_k. The distance between i_m and i, defined as $z_{i,i_m}(t) \equiv x_{i_m}(t) - x_i(t)$, is constrained by:

$$z_{i,i_m}(t_i^k) \geq \varphi v_i(t_i^k) + \delta, \quad \forall i \in S(t), \quad k \in \{1, 2, 3\} \tag{5}$$

where i_m can be determined and updated by the method described in section III-B.

We note that the rear-end safety constraint and the safe merging constraint take the time-to-collision into consideration, which is the most prevalent indicator used to identify collisions at roundabouts as reported, for example, in [31].

Constraint 3 (Lateral safety constraint) The moment generated by the centrifugal force needs to be smaller than the one generated by gravity in order to avoid rollover:

$$\kappa(x_i(t))v_i^2(t)h \leq w_h g \tag{6}$$

where h is the height of the CAV, w_h is the half width of the CAV (for simplicity, both assumed the same for all CAVs) and g is the gravity constant.

Constraint 4 (Vehicle limitations) The CAVs are also subject to velocity and acceleration constraints due to physical limitations or traffic rules:

$$\begin{aligned} v_{i,\min} \leq v_i(t) \leq v_{i,\max}, \forall t \in [t_i^0, t_i^f], \forall i \in S(t) \\ u_{i,\min} \leq u_i(t) \leq u_{i,\max}, \forall t \in [t_i^0, t_i^f], \forall i \in S(t) \end{aligned} \tag{7}$$

where $v_{i,\max} > 0$ and $v_{i,\min} \geq 0$ denote the maximum and minimum speed for CAV i, while $u_{i,\max} > 0$ and $u_{i,\min} < 0$ denote the maximum and minimum acceleration for CAV i. We further assume common speed limits dictated by the traffic rules at the roundabout, i.e. $v_{i,\min} = v_{\min}$, $v_{i,\max} = v_{\max}$.

Boundary conditions The initial position and velocity of the CAV as well as the terminal position are given as

$$x_i(t_i^0) = 0, v_i(t_i^0) = v_i^0, x_i(t_i^f) = L_i \tag{8}$$

where v_i^0 is the velocity of the CAV when entering the control zone CZ and L_i is the distance it needs to travel from its entry point to its assigned exit (L_i is determined once CAV i enters CZ.)

Similar to previous work [17], we construct a convex combination of the three objectives above:

$$J_i = \alpha_1 J_{i,1} + \alpha_2 \frac{J_{i,2}}{\frac{1}{2}\max\{u_{\max}^2, u_{\min}^2\}} + \alpha_3 \frac{J_{i,3}}{\kappa_{\max} v_{\max}^2} \tag{9}$$

where $\alpha_1, \alpha_2, \alpha_3 \in [0, 1]$, $\alpha_1 + \alpha_2 + \alpha_3 = 1$, $J_{i,2}$ and $J_{i,3}$ are properly normalized. Note that these weights are determined by each CAV according to its owner's relative preferences among time, energy, and comfort; they are set upon a CAV's arrival and remain unchanged during the CAV's trip. In particular, by defining $\beta_1 \equiv \frac{\alpha_1}{2\alpha_2}\max\{u_{\max}^2, u_{\min}^2\}$, $\beta_2 \equiv \frac{\alpha_3 \max\{u_{\max}^2, u_{\min}^2\}}{2\alpha_2 \kappa_{\max} v_{\max}^2}$, we can rewrite this minimization problem as

$$J_i(u_i) = \int_{t_i^0}^{t_i^f} \left(\beta_1 + \frac{1}{2}u_i^2(t) + \beta_2 \kappa(x_i(t))v_i^2(t)\right) dt \tag{10}$$

where β_1 and β_2 are the weight factors derived from α_1 and α_2. Finally, in what follows we simply choose in $J_{i,2}$ the quadratic function $C_i(u_i) = \frac{1}{2}u_i^2(t)$. Then, we can formulate the optimal control problem as follows:

Problem 1: For each CAV i following the dynamics (1), find the optimal control input $u_i(t)$ and terminal time t_i^f that minimizes (10) subject to constraints (1), (4), (5), (6), (6), (7), boundary conditions (8) and given t_i^0.

III. Decentralized Control Framework

In order to solve **Problem 1** for each CAV i, we need to first determine the corresponding i_p and i_m (when they exist) required in the safety constraints (4) and (5). Compared to the single-lane merging or intersection control problems where the constraints are determined and fixed immediately when CAV i enters the CZ, the main difficulty in a roundabout is that these constraints generally change after every event (defined earlier). In particular, for each CAV i at time t only the merging constraint related to the *next* MP ahead is considered. In other words, we need to determine at most one i_p to enforce (4) and one i_m to enforce (5) at any time instant.

There are two different ways to deal with this problem: (i) Treat the system as a single CZ with three MPs with advance knowledge of each CAV's sequence of MPs, or (ii) Decompose the roundabout into three separate merging problems corresponding to the three MPs, each with a separate CZ. The first approach heavily relies on the CAV sequencing policy used. If FIFO is applied, it is likely to perform poorly in a large roundabout, because a new CAV may experience a large delay in order to preserve the global FIFO passing sequence. In contrast, the second approach allows us to make use of the solution to the optimal merging problem [17] for each MP separately; it may, however, cause congestion if a roundabout is too small to provide adequate space for effective control at each separate CZ associated with each MP.

In what follows, we first address the task of determining the indices i_p and i_m for every CAV i in an event-driven manner which can be used in either of the two approaches above and for any desired sequencing policy. An extended queue table, an example of which is shown in Table I corresponding to Fig. 1, is used to record the essential state information and identify all conflicting CAVs. We specify the state-updating mechanism for this queue table so as to determine for each CAV i the corresponding i_p and i_m. Then, we focus on the second approach introduced above, and Section IV develops a general algorithm for solving **Problem 1** based on the OCBF method [15].

A. The Extended Coordinator Queue Table

Starting with the coordinator queue table shown in Fig. 1, we extend it to include 6 additional columns for each CAV i. The precise definitions are given below:

TABLE I
THE EXTENDED COORDINATOR QUEUE TABLE $S(t)$

$S(t)$								
idx	state	curr.	ori.	1st MP	2nd MP	3rd MP	i_p	i_m
0	$\boldsymbol{x}_0$	l_6	l_1	M_1, M	M_2, M	M_3, M		
1	$\boldsymbol{x}_1$	l_6	l_1	M_1, M	M_2, M	M_3, M	0	
2	$\boldsymbol{x}_2$	l_5	l_2	M_2, M				
3	$\boldsymbol{x}_3$	l_2	l_2	M_2	M_3	M_1		2
4	$\boldsymbol{x}_4$	l_2	l_2	M_2	M_3		3	
5	$\boldsymbol{x}_5$	l_3	l_3	M_3	M_1			1
6	$\boldsymbol{x}_6$	l_4	l_1	M_1, M				
7	$\boldsymbol{x}_7$	l_4	l_1	M_1, M	M_2	M_3	6	4
8	$\boldsymbol{x}_8$	l_1	l_1	M_1	M_2			7
9	$\boldsymbol{x}_9$	l_1	l_1	M_1	M_2	M_3	8	

- *idx*: Unique CAV index, which allows us to determine the order in which the CAV will leave the roundabout according to some policy (e.g., FIFO is assumed in Table I since rows are ordered by the index value).
- *state*: CAV state $\boldsymbol{x}_i = (x_i, v_i)$ where x_i denotes the distance from the entry point to the location of CAV i along its current road segment.
- *curr.*: Current CAV road segment, which allows us to determine the rear-end safety constraints.
- *ori.*: Original CAV road segment, which allows us to determine its relative position when in road segment *curr*.
- *1st-3rd MP*: These columns record all the MPs on the CAV trajectory. If a CAV has already passed an MP, this MP is marked with an "M". Otherwise, it is unmarked. This marker is used to systematically determine the safety constraints in Sec. III-B. As a CAV may not need to go through all three MPs in the roundabout, some of these columns may be blank.
- i_p: Index of the CAV that immediately precedes CAV i in the same road segment (if such a CAV exists).
- i_m: Index of the CAV that may conflict with CAV i at the next MP. CAV i_m is the last CAV that passes the MP ahead of CAV i. Note that if i_m and i are in the same road segment, then i_m $(= i_p)$ is the immediately preceding CAV. In this case, the safe merging constraint is redundant and need not be included.

Event-driven Update Process for $S(t)$: The extended coordinator queue table $S(t)$ is updated whenever an event (as defined earlier) occurs. In particular:

- A new CAV enters the CZ: The CAV is indexed and added to the bottom of the queue table.
- CAV i exits the CZ: All information of CAV i is removed. All rows with index larger than i decrease their index values by 1.
- CAV i passes an MP: Mark the MP with "M" and update the current road segment value *curr* of CAV i with the one it is entering.

Following each event, the values of i_p and i_m are also updated as detailed next.

B. Determination of Safety Constraints

Recall that for each CAV i in the CZ, we need to consider two different safety constraints (4) and (5). First, by looking at each row $j < i$ and the corresponding current road segment value *curr*, CAV i can determine its immediately preceding CAV i_p if one exists. This fully specifies the rear-end safety constraint (4).

Next, we determine i_m, the CAV (if it exists) which possibly conflicts with CAV i at the next MP it will pass so as to specify the safe merging constraint (5). To do so, we find in the extended queue table the last CAV $j < i$ that will pass or has passed the same MP as CAV i. In addition, if such a CAV is in the same road segment as CAV i, it coincides with the preceding CAV i_p. As an example, in Table I (a snapshot of Fig. 1), CAV 8 has no immediate preceding CAV in l_1, but it needs to yield to CAV 7 at M_1, its next MP: although CAV 7 has already passed M_1, when CAV 8 arrives at M_1 there needs to be adequate space between CAV 7 and 8 for CAV 8 to enter l_4). On the other hand, CAV 9 only needs to satisfy its rear-end safety constraint with CAV 8.

It is now clear that we can use the information in $S(t)$ in a systematic way to determine both i_p in (4) and i_m in (5). Thus, there are two functions $i_p(e)$ and $i_m(e)$ which need to be updated after event e if this event affects CAV i. First, the index i_p can be easily determined by looking at rows $j < i$, starting at row i and moving up in the list, until the first one is found with the same value *curr* as CAV i. For example, CAV 9 searches for its i_p from CAV 8 to the top and sets $i_p = 8$ as CAV 8 has the *curr* value l_1.

Next, the index i_m is determined. To do this, CAV i compares its MP information to that of each CAV in rows $j < i$, starting at row i and moving up in the list. The process terminates the first time that any one of the following two conditions is satisfied:

- The MP information of CAV j *matches* CAV i. We define j to "match" i if and only if the last marked MP or the first unmarked MP of CAV j is the same as the first unmarked MP of CAV i. Thus, $i_m = j$.
- All prior rows $j < i$ have been looked up and none of them matches the MP information of CAV i.

Combining the two updating processes for i_p and i_m together, there are four different cases as follows:

1. Both i_p and i_m exist. In this case, there are two possibilities: (i) $i_p \neq i_m$. CAV i has to satisfy the safe merging constraint (5) with $i_m < i$ and also satisfy the rear-end safety constraint (4) with $i_p < i$. For example, for $i = 7$, we have $i_p = 6$ and $i_m = 4$ (M_2 is the first unmarked MP for CAV 7 and that matches the first unmarked MP for CAV 4). (ii) $i_p = i_m$. CAV i only has to follow i_p and satisfy the rear-end safety constraint (4) with respect to i_p. Thus, there is no safe merging constraint for CAV i to satisfy. For example, $i = 4$ and $i_p = i_m = 3$.

2. Only i_p exists. In this case, there is no safe merging constraint for CAV i to satisfy. CAV i only needs to follow the preceding CAV i_p and satisfy the rear-end safety constraint (4) with respect to i_p. For example, $i = 1$ and $i_p = 0$.

3. Only i_m exists. In this case, CAV i has to satisfy the safe merging constraint (5) with the CAV i_m in $S(t)$. There is no preceding CAV i_p, thus there is no rear-end safety constraint. For example, $i = 5$ and $i_m = 1$ (M_3 is the first unmarked MP for CAV 5 and that matches the last marked MP for CAV 1 with no other match for $j = 4, 3, 2$).

4. Neither i_p nor i_m exists. In this case, CAV i does not have to consider any safety constraints. For example, $i = 2$.

C. Sequencing Policies Using Local Coordinator Queue Tables

The extended queue table $S(t)$ is based on a sequencing policy which applies to the whole roundabout. Thus, if a FIFO policy is adopted, we have seen how to use a systematic process for updating $i_p(e)$ and $i_m(e)$ after each event e in $S(t)$. However, FIFO may not be a good sequencing policy if applied to the whole roundabout. More generally, we wish to allow possible resequencing after a CAV passes a MP, based on the system state information at that time. This can be accomplished by introducing a *local* coordinator queue table $S_k(t)$ associated with each M_k, $k = 1, 2, 3$. This allows us to treat the problem of coordinating all CAVs with M_k as their next (or just passed) MP as a separate optimal merging control problem along the lines of [17]. We define CZ_k as the CZ corresponding to M_k that consists of the three road segments directly connected to M_k. A local coordinator queue table can be viewed as a subset of the extended coordinator queue table except that the CAVs appear in a different order in the two tables. As an example, Table II (a snapshot of Fig. 1) is the local coordinator queue table corresponding to M_1 (in this case, for simplicity, we still use the FIFO policy, but it is now applied only to CAVs involved with M_1).

TABLE II
THE LOCAL-COORDINATOR QUEUE TABLE $S_1(t)$

$S_1(t)$								
idx	info	curr.	ori.	1st MP	2nd MP	3rd MP	i_p	i_m
6	$\boldsymbol{x}_6$	l_4	l_1	M_1, M				
7	$\boldsymbol{x}_7$	l_4	l_1	M_1, M	M_2	M_3	6	
8	$\boldsymbol{x}_8$	l_1	l_1	M_1	M_2			7
0	$\boldsymbol{x}_0$	l_6	l_1	M_1, M	M_2, M	M_3, M		
1	$\boldsymbol{x}_1$	l_6	l_1	M_1, M	M_2, M	M_3, M	0	
9	$\boldsymbol{x}_9$	l_1	l_1	M_1	M_2	M_3	8	

Event-driven Update Process for $S_k(t)$: The local-coordinator queue table $S_k(t)$ is updated as follows after each event that has caused an update of the extended coordinator queue table $S(t)$:

- For each CAV i in $S_k(t)$, update its information depending on the event observed: (i) A new CAV j enters CZ_k (either from an entry point to the roundabout CZ or a MP passing event): Add a new row to $S_k(t)$ and resequence the local-coordinator queue table according to the sequencing policy used. (ii) CAV j exits CZ_k: Remove all the information of CAV j from $S_k(t)$.
- Determine i_p and i_m in each local-coordinator queue table with the same method as described in section III-B.
- Update CAV j's i_p and i_m in the extended coordinator queue table with the corresponding information in $S_k(t)$, while M_k is the next MP of CAV j.

Note that CAV j may appear in multiple local-coordinator queue tables with different i_p and i_m values. However, only the one in $S_k(t)$ where M_k is the next MP CAV j will pass is used to update the extended coordinator queue table $S(t)$. The information of CAV j in other local-coordinator queue tables is necessary for determining the safety constraints as CAV j may become CAV i_p or i_m of other CAVs.

Resequencing policy: The local-coordinator queue table allows resequencing when a CAV passes a MP. A resequencing policy evaluates a given criterion for each CAV and sorts the CAVs in the queue table when a new event happens. For example, FIFO takes the arrival time in the CZ as the criterion, while the Dynamic Resequencing (DR) policy [28] uses the overall objective value in (10) as the criterion.

We propose here a straightforward yet effective resequencing policy for the roundabout as follows. Let $\tilde{x}_i^k \equiv x_i - d_j^k$ be the position of CAV i relative to M_k, where d_j^k denotes the fixed distance from the entry point (origin) O_j to merging point M_k along the trajectory of CAV i. Then, consider

$$y_i(t) = -\tilde{x}_i^k(t) \tag{11}$$

This resequencing criterion reflects the distance between the CAV and the next MP. The CAV which has the smallest $y_i(t)$ value is allocated first, thus this is referred to as the *Shortest Distance First* (SDF) policy. This simple resequencing policy is tested in Section VI. Other policies can also be easily implemented with the help of the local-coordinator queue tables.

IV. Unconstrained Optimal Control Solution

We now return to the solution of **Problem 1**, i.e., the minimization of (10) subject to constraints (1), (4), (5), (7), (6), the initial condition $x_i(t_i^0) = 0$, and given t_i^0, v_i^0 and $x_i(t_i^f)$. The problem formulation is complete since we have used the local coordinator queue tables to determine i_p and i_m (needed for the safety constraints) associated with the closest MP to CAV i.

As pointed out in [17], when one or more constraints become active, the solution to **Problem 1** becomes computationally intensive. The problem here is exacerbated by the fact that the values of i_p and i_m dynamically change due to different events in the roundabout system. To ensure that a solution can be obtained in real time while also *guaranteeing that all safety constraints are always satisfied*, we adopt the OCBF approach [15] briefly introduced in the introduction and further discussed in Section V: we first determine the solution of the *unconstrained* optimal control problem and then solve a problem of optimally tracking this solution while guaranteeing the satisfaction of all constraints through the use of Control Barrier Functions (CBFs).

Thus, our first task is to obtain a solution to the unconstrained roundabout problem through Hamiltonian analysis. Denoting by $\mathcal{X}_i(t) := (x_i(t), v_i(t))$ and $\lambda_i(t) := (\lambda_i^x(t), \lambda_i^v(t))$ the state vector and costate vector respectively, the Hamiltonian of the system in (10) is

$$\begin{aligned}\mathcal{H}_i(\mathcal{X}_i, \lambda_i, u_i) =& \beta_1 + \frac{1}{2}u_i^2 + \beta_2\kappa(x_i)v_i^2 + \lambda_i^x v_i + \lambda_i^v u_i \\ &+ \mu_i^a(u_i - u_{\max}) + \mu_i^b(u_{\min} - u_i) \\ &+ \mu_i^c(v_i - v_{\max}) + \mu_i^d(v_{\min} - v_i) \\ &+ \mu_i^e(x_i + \varphi v_i + \delta - x_{i_p}) \\ &+ \mu_i^f(\kappa(x_i)v_i^2 h - w_h g)\end{aligned} \tag{12}$$

where $\mu_i^a, \mu_i^b, \mu_i^c, \mu_i^d, \mu_i^e, \mu_i^f$ are Lagrange multipliers associated with the constraints (4), (5), (7) and (6). Since the terminal state constraint $\psi_{i,1} := x_i(t_i^f) - L_i = 0$ is not an explicit function of time, the transversality condition is

$$H_i(\mathcal{X}_i(t), \lambda_i(t), u_i(t))|_{t=t_i^f} = 0 \tag{13}$$

The necessary conditions for optimality are

$$\dot{\lambda}_i^x = -\frac{\partial \mathcal{H}_i}{\partial x_i} = -\mu_i^e - \beta_2\frac{\partial\kappa(x_i)}{\partial x_i}v_i^2 - \mu_i^f\frac{\partial\kappa(x_i)}{\partial x_i}v_i^2 \tag{14}$$

$$\begin{aligned}\dot{\lambda}_i^v = -\frac{\partial \mathcal{H}_i}{\partial v_i} =& -2\beta_2\kappa(x_i)v_i - \lambda_i^x - (\mu_i^c - \mu_i^d) \\ &- \varphi\mu_i^e - 2\kappa(x_i)\mu_i^f v_i\end{aligned} \tag{15}$$

$$0 = \frac{\partial \mathcal{H}_i}{\partial u_i} = u_i + \lambda_i^v + \mu_i^a - \mu_i^b \tag{16}$$

Under the unconstrained assumption, none of the constraints (4), (5), (7) and (6) is active, therefore, $\mu_i^a = \mu_i^b = \mu_i^c = \mu_i^d = \mu_i^e = \mu_i^f = 0$. Then, the most complex part in solving the equations above is due to $\frac{\partial\kappa(x_i)}{\partial x_i}$ appearing in (14). In [32], a single curved road segment was modeled by assuming $\kappa(x_i)$ to be a constant taken to be the average curvature $\bar{\kappa}$ or the maximum curvature $\kappa_{\max}$. However, in a roundabout road configuration, we cannot take $\kappa(x_i)$ to be a constant over an entire CAV trajectory, but rather define it as a piecewise constant function which is 0 when $x_i \in [0, L)$ and jumps to $1/r$ at $x_i = L$. This discontinuity in $\kappa(x_i)$ causes complications in (14).

There are several ways to deal with this discontinuity problem in $\kappa(x_i)$. For example, one can approximate it through a smooth (e.g., sigmoid) function. However, even the simplest sigmoid function results in a set of complex nonlinear equations too hard to solve in real time. In what follows, we resolve this issue by transforming **Problem 1** into a bi-level optimal control problem as described next.

At the lower level, we separate the problem for each CAV i into two parts: one for the straight road segment and one for the circular part. Both problems are parameterized by the terminal speed of CAV i, v_i^m, at the end of the straight road segment, which is also the initial speed for the circular part. Then, the upper level problem consists of determining an optimal value for the parameter v_i^m.

To formulate the two lower-level problems, let t_i^m be the time a CAV enters the circular part of the roundabout from the straight road segment. The boundary conditions for the speed of CAV i when entering the straight road segment and the circular part are v_i^0 and v_i^m respectively. Then, we formulate the two *lower-level problems* corresponding to the straight line and the circular part (both parameterized by v_i^m) as follows:

$$\begin{aligned}&\min_{u_i(t)} J_i^{\mathrm{S}}(u_i(t); v_i^m) = \int_{t_i^0}^{t_i^m} f_i^{\mathrm{S}}(u_i(t))dt \\ &s.t.\ \ (1), (4), (5), (7) \\ &\qquad v_i(t_i^0) = v_i^0, v_i(t_i^m) = v_i^m \\ &\qquad x_i(t_i^m) = 0, x_i(t_i^f) = L_{i,1}\end{aligned} \tag{17}$$

$$\begin{aligned}&\min_{u_i(t)} J_i^{\mathrm{C}}(u_i(t); v_i^m) = \int_{t_i^m}^{t_i^f} f_i^{\mathrm{C}}(u_i(t), \boldsymbol{v}_i(t))dt \\ &s.t.\ \ (1), (4), (5), (7), (6) \\ &\qquad v_i(t_i^m) = v_i^m \\ &\qquad x_i(t_i^m) = L_{i,1}, x_i(t_i^f) = L_i\end{aligned} \tag{18}$$

where, for notational simplicity, we have defined

$$f_i^{\mathrm{S}}(u_i(t)) = \beta_1 + \frac{1}{2}u_i^2(t)$$

$$f_i^{\mathrm{C}}(u_i(t), \boldsymbol{v}_i(t)) = \beta_1 + \frac{1}{2}u_i^2(t) + \beta_2\kappa v_i^2(t)$$

Note that f_i^{S} and f_i^{C} are both special cases of the integrand in (10). In f_i^{S} the curvature is $\kappa(x_i) = 0$, while in f_i^{C} the curvature is a constant $\kappa(x_i) = \hat{\kappa}$. Given the speed parameter v_i^m, solving the lower level problems yields two optimal costs $J_i^{*\mathrm{S}}(v_i^m)$ and $J_i^{*\mathrm{C}}(v_i^m)$, both functions of v_i^m. We then formulate the following *upper level problem* which aims at finding the optimal terminal velocity v_i^m:

$$\begin{aligned}&\min_{v_i^m} J_i(v_i^m) = J_i^{*\mathrm{S}}(v_i^m) + J_i^{*\mathrm{C}}(v_i^m) \\ &s.t.\ \ v_{\min} \le v_i^m \le v_{\max}\end{aligned} \tag{19}$$

A. Lower level problem 1 – Circular road segment

The circular part problem is a special case of **Problem 1** where the curvature $\kappa(x_i)$ is constant, i.e. $\kappa = \hat{\kappa}$. Under the unconstrained assumption, $\mu_i^a = \mu_i^b = \mu_i^c = \mu_i^d = \mu_i^e = \mu_i^f = 0$ and the necessary conditions (14), (15), (16) yield:

$$\dot{\lambda}_i^x = -\frac{\partial \mathcal{H}_i}{\partial x_i} = 0 \tag{20}$$

$$\dot{\lambda}_i^v = -\frac{\partial \mathcal{H}_i}{\partial v_i} = -2\beta_2\hat{\kappa}v_i - \lambda_i^x \tag{21}$$

$$0 = \frac{\partial \mathcal{H}_i}{\partial u_i} = u_i + \lambda_i^v \tag{22}$$

Since (20) implies that λ_i^x is a constant, set $\lambda_i^x = a_i$. Then, combining (21) and (22) yields

$$\ddot{v_i} - 2\beta_2\hat{\kappa}v_i - a_i = 0 \tag{23}$$

Solving this equation gives an explicit solution for the speed:

$$v_i^*(t) = b_i e^{\sqrt{2\beta_2\hat{\kappa}}t} + c_i e^{-\sqrt{2\beta_2\hat{\kappa}}t} - \frac{a_i}{2\beta_2\hat{\kappa}} \tag{24}$$

where b_i, c_i are integration constants. Applying (1), the optimal solution for the unconstrained problem is obtained as follows:

$$u_i^*(t) = \sqrt{2\beta_2\kappa}(b_i e^{\sqrt{2\beta_2\hat{\kappa}}t} - c_i e^{-\sqrt{2\beta_2\hat{\kappa}}t}) \tag{25}$$

$$x_i^*(t) = \frac{1}{\sqrt{2\beta_2\kappa}}(b_i e^{\sqrt{2\beta_2\hat{\kappa}}t} - c_i e^{-\sqrt{2\beta_2\hat{\kappa}}t}) - \frac{a_i}{2\beta_2\kappa}t + d_i \tag{26}$$

where d_i is also an integration constant.

Given the boundary conditions $v_i(t_i^m) = v_i^m$, $x_i(t_i^m) = L_{i,1}$, $\lambda_i^v(t_i^f) = 0$, $x_i(t_i^f) = L_i$, as well as the transversality condition (13), we can obtain a_i, b_i, c_i, d_i and t_i^f by solving the set of nonlinear algebraic equations:

$$\begin{aligned}
&b_i e^{\sqrt{2\beta_2\hat{\kappa}}t_i^m} + c_i e^{-\sqrt{2\beta_2\hat{\kappa}}t_i^m} - \frac{a_i}{2\beta_2\hat{\kappa}} = v_i^m \\
&\frac{1}{\sqrt{2\beta_2\hat{\kappa}}}(b_i e^{\sqrt{2\beta_2\hat{\kappa}}t_i^m} - c_i e^{-\sqrt{2\beta_2\hat{\kappa}}t_i^m}) - \frac{a_i}{2\beta_2\kappa}t_i^m + d_i = L_{i,1} \\
&\frac{1}{\sqrt{2\beta_2\hat{\kappa}}}(b_i e^{\sqrt{2\beta_2\hat{\kappa}}t_i^f} - c_i e^{-\sqrt{2\beta_2\hat{\kappa}}t_i^f}) - \frac{a_i}{2\beta_2\kappa}t_i^f + d_i = L_i \\
&\sqrt{2\beta_2\hat{\kappa}}(b_i e^{\sqrt{2\beta_2\hat{\kappa}}t_i^f} - c_i e^{-\sqrt{2\beta_2\hat{\kappa}}t_i^f}) = 0 \\
&\beta_1 + \beta_2\hat{\kappa}(b_i e^{\sqrt{2\beta_2\hat{\kappa}}t_i^f} + c_i e^{-\sqrt{2\beta_2\hat{\kappa}}t_i^f} - \frac{a_i}{2\beta_2\hat{\kappa}})^2 \\
&\qquad + a_i(b_i e^{\sqrt{2\beta_2\hat{\kappa}}t_i^f} + c_i e^{-\sqrt{2\beta_2\hat{\kappa}}t_i^f} - \frac{a_i}{2\beta_2\hat{\kappa}}) = 0
\end{aligned} \tag{27}$$

Thus, by solving (27) for each $i \in S(t)$, we can obtain all the integration constants a_i, b_i, c_i, d_i and the terminal time t_i^f for CAV i as a function of v_i^m. Since (27) is usually hard to solve due to the presence of the exponential terms, we will present in Section IV-C a computationally efficient approach to calculate these five constants, as well as the optimal cost.

B. Lower level problem 2 – Straight road segment

In this case, the Hamiltonian in (12) becomes

$$\begin{aligned}
\mathcal{H}_i(\mathcal{X}_i, \lambda_i, u_i) =& \beta_1 + \frac{1}{2}u_i^2 + \lambda_i^x v_i + \lambda_i^v u_i \\
&+ \mu_i^a(u_i - u_{\max}) + \mu_i^b(u_{\min} - u_i) \\
&+ \mu_i^c(v_i - v_{\max}) + \mu_i^d(v_{\min} - v_i) \\
&+ \mu_i^e(x_i + \varphi v_i + \delta - x_{i_p})
\end{aligned} \tag{28}$$

with the transverality condition

$$\mathcal{H}_i(\mathcal{X}_i, \lambda_i, u_i)|_{t=t_i^m} = 0 \tag{29}$$

The necessary conditions for optimality are

$$\dot{\lambda}_i^x = -\frac{\partial \mathcal{H}_i}{\partial x_i} = -\mu_i^e \tag{30}$$

$$\dot{\lambda}_i^v = -\frac{\partial \mathcal{H}_i}{\partial v_i} = -\lambda_i^x - (\mu_i^c - \mu_i^d) - \varphi\mu_i^e \tag{31}$$

$$0 = \frac{\partial \mathcal{H}_i}{\partial u_i} = u_i + \lambda_i^v + \mu_i^a - \mu_i^b \tag{32}$$

Again, under the unconstrained assumption, $\mu_i^a = \mu_i^b = \mu_i^c = \mu_i^d = \mu_i^e = 0$. Therefore, solving the equations above, we can explicitly obtain the optimal solution to the unconstrained problem as:

$$\begin{aligned}
u_i^*(t) &= a_i t + b_i \\
v_i^*(t) &= \frac{1}{2}a_i t^2 + b_i t + c_i \\
x_i^*(t) &= \frac{1}{6}a_i t^3 + \frac{1}{2}b_i t^2 + c_i t + d_i
\end{aligned} \tag{33}$$

The boundary conditions for this problem are $v_i(t_i^0) = v_i^0$, $v_i(t_i^m) = v_i^m$, $x_i(t_i^0) = 0$ and $x_i(t_i^m) = L_{i,1}$. Combining these boundary conditions with the tranversality condition (29) yields the following set of equations from which all the integration constants a_i, b_i, c_i, d_i and the terminal time t_i^m can be obtained, again as a function of v_i^m:

$$\begin{aligned}
&\frac{1}{2}a_i \cdot (t_i^0)^2 + b_i \cdot t_i^0 + c_i = v_i^0, \\
&\frac{1}{2}a_i \cdot (t_i^m)^2 + b_i \cdot t_i^0 + c_i = v_i^m, \\
&\frac{1}{6}a_i \cdot (t_i^0)^3 + \frac{1}{2}b_i \cdot (t_i^0)^2 + c_i t_i^0 + d_i = 0, \\
&\frac{1}{6}a_i \cdot (t_i^m)^3 + \frac{1}{2}b_i \cdot (t_i^m)^2 + c_i t_i^m + d_i = L, \\
&\beta - \frac{1}{2}b_i^2 + a_i c_i = 0.
\end{aligned} \tag{34}$$

This set equations is not difficult to solve; in practice, the solution can be obtained within $\ll 1$s using MATLAB.

C. The upper level problem

Once the solution $u_i^*(t)$ in (33) is obtained in conjunction with (34), we have the optimal cost $J_i^{*\mathrm{S}}(v_i^m)$ available in (19). Similarly, once $v_i^*(t)$ and $u_i^*(t)$ in (24) and (25) are obtained in conjunction with (27), then $J_i^{*\mathrm{C}}(v_i^m)$ is available and (19) becomes a standard nonlinear programming problem whose solution gives an optimal v_i^m. The difficulty, however, is that explicit analytical expressions for $J_i^{*\mathrm{S}}(v_i^m)$ and $J_i^{*\mathrm{C}}(v_i^m)$ are

generally unavailable. The numerical evaluation of these two terms, given a particular v_i^m value, is computationally expensive and this is especially true for $J_i^{*\mathrm{C}}(v_i^m)$ where exponential terms are involved. A straightforward and intuitive way to solve the upper level problem in real time is to use a regression approach to obtain explicit expressions for the two optimal cost functions. This provides a computationally efficient solution at the expense of some accuracy in determining the optimal v_i^m.

What is important to note is that the aforementioned regression approach can be carried out *off line*. To explain this, let us consider the first lower-level problem for the circular part. For any CAV i with a given origin and destination, the physical parameter values of $L_{i,1}$, L_i and $\hat{\kappa}$ in (18) are fixed. Therefore, given the parameters β_1, β_2, for any fixed v_i^m, a shift in the arrival time t_i^m will only result in a shift in the optimal control but does not influence the optimal travel time or the optimal cost. In other words, for $i, j \in S(t)$, if $v_i^m = v_j^m$ and $\Delta t = t_j^m - t_i^m$, we have $u_i^*(t) = u_j^*(t + \Delta t)$ as well as $t_i^f - t_i^m = t_j^f - t_j^m$. It follows that

$$\begin{aligned} J_i^{*\mathrm{C}}(v_i^m) &= \int_{t_i^m}^{t_i^f} f_i^{\mathrm{C}}(u_i^*(t), \boldsymbol{x}_i^*(t))dt \\ &= \int_{t_i^m+\Delta t}^{t_i^f+\Delta t} f_j^{\mathrm{C}}(u_j^*(t), \boldsymbol{x}_j^*(t))dt = J_j^{*,\mathrm{C}}(v_j^m) \end{aligned} \tag{35}$$

where $f_i^{\mathrm{C}}(u(t), x(t)) = f_j^{\mathrm{C}}(u(t), x(t))$ for given β_1 and β_2. This implies that the optimal cost function $J_i^{*,\mathrm{C}}(v_i^m)$ is independent of the initial time t_i^m. Therefore, given β_1, β_2 for a roundabout with physical parameters $\hat{\kappa}, L_{i,1}$ and L_i, we can get the optimal cost $J_i^{*\mathrm{C}}(v_i^m)$ for any fixed $v_i^m \in [v_i^{\min}, v_i^{\max}]$ by solving (27) off line with $t_i^m = 0$. Following this approach, we can calculate a number of optimal cost and initial speed pairs $(J_i^{*\mathrm{C}}(v_i^m), v_i^m)$ off line and use any standard regression method to fit the optimal cost function:

$$\mathcal{R}_J^C(v_i^m) = J_i^{*\mathrm{C}}(v_i^m) + \epsilon(v_i^m) \tag{36}$$

where $\mathcal{R}_J^C : \mathbb{R} \to \mathbb{R}$ denotes the regression model for the optimal cost, and ϵ denotes the regression error.

Using the same technique, another regression model $\mathcal{R}_J^S(v_i^m)$ can be calculated off line as an approximation to the optimal cost function $J_i^{*\mathrm{S}}(v_i^m)$ for CAV i in the straight road segment. Thus, the objective function of the upper level problem can be explicitly expressed by the regression model:

$$J_i(v_i^m) = \mathcal{R}_J^S(v_i^m) + \mathcal{R}_J^C(v_i^m) \tag{37}$$

Then, the upper-level problem becomes a nonlinear programming problem with an explicit objective function. This is usually easy to solve and the optimal v_i^m is readily obtained in real time.

Once the optimal velocity v_i^m is determined, the explicit solution of the two lower-level optimal control problems can be obtained by solving (27) and (34) respectively. Regarding (27), as mentioned in Section IV-A, a solution can be computationally expensive to obtain due to the exponential terms involved. To accelerate this solution process, we can eliminate the variable t_i^f in (27), hence obtaining a much simpler system of only four equations to solve; this is accomplished by employing a similar regression technique for t_i^f in terms of v_i^m as explained next.

As already pointed out, for a specific roundabout where $L_{i,1}$ and L_i are fixed, the total travel time $t_i^f - t_i^m$ is independent of the arrival time t_i^m. Thus, given β_1, β_2 and the physical parameters $\hat{\kappa}, L_{i,1}$ and L_i, we can calculate a number of travel time and initial speed pairs $(t_i^f - t_i^m, v_i^m)$ off line for any fixed v_i^m. A regression model $\mathcal{R}_t^C(v_i^m)$ is then used to fit the travel time as follows:

$$\mathcal{R}_t^C(v_i^m) = (t_i^f - t_i^m) + \epsilon(v_i^m) \tag{38}$$

where $\mathcal{R}_t : \mathbb{R} \to \mathbb{R}$ denotes the regression model for the optimal travel time and $\epsilon(v_i^m)$ represents the regression error. Thus, for any observed initial velocity $v_i^m \in [v_{\min}, v_{\max}]$, we can use this regression model to obtain the solution of t_i^f:

$$t_i^f = t_i^m + \mathcal{R}_t^C(v_i^m) \tag{39}$$

Given β_1, β_2 and v_i^m and the regression model $\mathcal{R}_t^C(v_i^m)$, the optimal terminal time can be immediately obtained using (39). Therefore, the problem (18) is reduced into an optimal control problem with fixed terminal time. The transversality condition (the last equation in (27)) is no longer needed. Then, the integration constants can be obtained easily and quickly through a simple matrix multiplication:

$$\begin{bmatrix} a_i \\ b_i \\ c_i \\ d_i \end{bmatrix} = \begin{bmatrix} -\frac{1}{2\beta_2\hat{\kappa}} & e^{\sqrt{2\beta_2\hat{\kappa}}t_i^m} & e^{-\sqrt{2\beta_2\hat{\kappa}}t_i^m} & 0 \\ -\frac{1}{2\beta_2\hat{\kappa}} & \frac{e^{\sqrt{2\beta_2\hat{\kappa}}t_i^m}}{2\beta_2\hat{\kappa}} & -\frac{e^{-\sqrt{2\beta_2\hat{\kappa}}t_i^m}}{2\beta_2\hat{\kappa}} & 1 \\ -\frac{1}{2\beta_2\hat{\kappa}} & \frac{e^{\sqrt{2\beta_2\hat{\kappa}}t_i^f}}{2\beta_2\hat{\kappa}} & -\frac{e^{-\sqrt{2\beta_2\hat{\kappa}}t_i^f}}{2\beta_2\hat{\kappa}} & 1 \\ 0 & e^{\sqrt{2\beta_2\hat{\kappa}}t_i^f} & e^{-\sqrt{2\beta_2\hat{\kappa}}t_i^f} & 0 \end{bmatrix}^{-1} \begin{bmatrix} v_i^m \\ L_{i,1} \\ L_i \\ 0 \end{bmatrix} \tag{40}$$

Although (34) for the second lower-level problem is easy to solve, the solution can still be accelerated by a similar regression approach: a number of travel time pairs $(t_i^m - t_i^0, v_i^m)$ can be calculated off line to generate a regression model:

$$\mathcal{R}_t^S(v_i^m) = (t_i^m - t_i^0) + \epsilon(v_i^m) \tag{41}$$

which efficiently calculates the optimal terminal time. This reduces (34) to only four equations which are easily and quickly solved by a matrix multiplication:

$$\begin{bmatrix} a_i \\ b_i \\ c_i \\ d_i \end{bmatrix} = \begin{bmatrix} \frac{1}{2}(t_i^0)^2 & t_i^0 & 1 & 0 \\ \frac{1}{2}(t_i^m)^2 & t_i^m & 1 & 0 \\ \frac{1}{6}(t_i^0)^3 & \frac{1}{2}(t_i^0)^2 & t_i^0 & 1 \\ \frac{1}{6}(t_i^m)^3 & \frac{1}{2}(t_i^m)^2 & t_i^m & 1 \end{bmatrix}^{-1} \begin{bmatrix} v_i^0 \\ v_i^m \\ 0 \\ L \end{bmatrix} \tag{42}$$

V. Joint optimal control and control barrier function controller (OCBF)

In Sec. IV, the optimal solution to **Problem 1** with all constraints inactive was obtained. This solution forms the basis of the OCBF approach [15]: (i) the solution for the *unconstrained* optimal control problem is used as a reference control, (ii) the resulting control reference trajectory is optimally tracked subject to the bounds (7), as well as a set of CBF constraints enforcing (4), (5) and (6) (iii) This optimal tracking problem is efficiently solved by discretizing time and solving a simple Quadratic Problem (QP) at each discrete time

step. The significance of CBFs in this approach is twofold: first, their forward invariance property [15] guarantees that all constraints they enforce are satisfied at all times if they are initially satisfied; second, CBFs impose *linear* constraints on the control which is what enables the efficient solution of the tracking problem through the sequence of QPs in (iii) above.

Once we obtain the unconstrained optimal control solution for the straight (33) and circular road segment (25) respectively, we define it as a control reference trajectory $u_{ref}(t)$. More generally, we can define any function $h(u_i^*(t), x_i^*(t), x_i(t))$ as a control reference $u_{ref}(t) = h(u_i^*(t), x_i^*(t), x_i(t))$, where $x_i(t)$ provides feedback from the actual observed CAV trajectory to add robustness to the solution. We normally choose the simplest and most straightforward choice $u_{ref}(t) = u_i^*(t)$ where $u_i^*(t)$ is the unconstrained optimal control solution obtained from (33) and (25). We will, however, revisit the case with feedback in Section V-A.

Next, we design a controller that optimally tracks $u_{ref}(t)$ while satisfying all constraints. First, let $\boldsymbol{x}_i(t) \equiv (x_i(t), v_i(t))$. Based on the vehicle dynamics (1), define $f(\boldsymbol{x}_i(t)) = [v_i(t), 0]^T$ and $g(\boldsymbol{x}_i(t)) = [0, 1]^T$. Each of the constraints (4), (5) and (7) is expressed in the form $b_k(\boldsymbol{x}_i(t)) \geq 0, k \in \{1, ..., n\}$ where n is the number of constraints. The CBF method maps a constraint $b_k(\boldsymbol{x}_i(t)) \geq 0$ onto a new constraint which directly involves the control $u_i(t)$ in *linear* fashion and takes the general form

$$L_f b_k(\boldsymbol{x}_i(t)) + L_g b_k(\boldsymbol{x}_i(t)) u_i(t) + \gamma(b_k(\boldsymbol{x}_i(t))) \geq 0, \quad (43)$$

where L_f, L_g denote the Lie derivatives of $b_k(\boldsymbol{x}_i(t))$ along f and g respectively and $\gamma(\cdot)$ denotes any class-$\mathcal{K}$ function [15]. The forward invariance property of CBFs guarantees that a control input that keeps (43) satisfied will also keep $b_k(\boldsymbol{x}_i(t)) \geq 0$. In other words, the constraints (4), (5), (7) and (6) are never violated (this comes at the expense of potential conservativeness in the control since the CBF constraint is a sufficient condition for ensuring its associated original problem constraint.)

Considering all constraints in **Problem 1**, the rear-end safety constraint (4), the vehicle limitations (7) and the lateral safety constraint (6) are all straightforward to transform into a CBF form by directly applying (43). As an example, consider (4) by setting $b_1(\boldsymbol{x}_i(t)) = z_{i,i_p}(t) - \varphi v_i(t) - \delta = x_{i_p}(t) - x_i(t) - \varphi v_i(t) - \delta$. As $b_1(\boldsymbol{x}_i(t))$ is differentiable, we can calculate the Lie derivatives $L_f b_1(\boldsymbol{x}_i(t)) = v_{i_p} - v_i$ and $L_g b_1(\boldsymbol{x}_i(t)) = -\varphi$. Choosing a linear class-$\mathcal{K}$ function $\gamma(x) = k_1 x$, the CBF constraint (43) can be obtained as

$$b_{\text{cbf}_1}(\boldsymbol{x}_i, u_i) = v_{i_p} - v_i - \varphi u_i + k_1 b_1(\boldsymbol{x}_i) \geq 0 \quad (44)$$

The safe merging constraint (5) differs from the rest in that it only applies to a single specific time instants $t_i^{m_k}$. This poses a technical complication due to the fact that a CBF must always be in a continuously differentiable form. We can convert (5) to such a form using the technique in [15] to obtain

$$z_{i,i_m}(t) - \Phi(x_i(t)) v_i(t) - \delta \geq 0, \quad t \in [t_i^{k,0}, t_i^k] \quad (45)$$

where $t_i^{k,0}$ denotes the time CAV i enters the road segment connected to M_k and $\Phi(\cdot)$ is any strictly increasing function as long as it satisfies the boundary constraints $z_{i,i_m}(t_i^{k,0}) - \phi v_i(t_i^{k,0}) - \delta \geq 0$ and $z_{i,i_m}(t_i^k) - \phi v_i(t_i^k) - \delta \geq 0$ (the latter is precisely (5)). Note that we need to satisfy (45) when a CAV changes road segments in the roundabout and the value of i_m changes. Since $z_{i,i_m}(t_i^{k,0}) \geq -L_{i_m} + L_i$, where L_i is the length of the road segment CAV i is in, to guarantee the feasibility of (45), we set $\Phi(x_i(t_i^{k,0})) v_i(t_i^{k,0}) + \delta = -L_{i_m} + L_i$. Then, from (5), we get $\Phi(x_i(t_i^k)) = \varphi$. Simply choosing a linear $\Phi(\cdot)$ as follows:

$$\Phi(x_i(t)) = \left(\varphi + \frac{L_{i_m} - L_i + \delta}{v_i(t_i^{k,0})}\right) \frac{x_i(t)}{L_i} - \frac{L_{i_m} - L_i + \delta}{v_i(t_i^{k,0})} \quad (46)$$

it is easy to check that it satisfies the boundary requirements. Note that when implementing the OCBF controller, $x_i(t)$ needs to be transformed into a relative position $\tilde{x}_i^k + L_i$, which reflects the distance between CAV i and the origin of the current road segment. Thus, z_{i,i_p} and z_{i,i_m} are calculated after this transformation, where $z_{i,i_p} = \tilde{x}_{i_p}^k - \tilde{x}_i^k$, $z_{i,i_m} = \tilde{x}_{i_m}^k - \tilde{x}_i^k$.

The last step is to provide the OCBF controller with the capability to optimally track the reference speed trajectory. This is accomplished by using a Control Lyapunov Function (CLF) $V(\boldsymbol{x}_i(t))$ which is similar to a CBF. Letting $V(\boldsymbol{x}_i(t)) = (v_i(t) - v_{ref}(t))^2$, the CLF constraint takes the form

$$L_f V(\boldsymbol{x}_i(t)) + L_g V(\boldsymbol{x}_i(t)) u_i(t) + \epsilon V(x_i(t)) \leq e_i(t), \quad (47)$$

where $\epsilon > 0$, and $e_i(t)$ is a relaxation variable which makes this a soft constraint.

We can now formulate the problem that the OCBF controler must solve, i.e., to optimally track the reference trajectory by solving the optimization problem:

$$\min_{u_i(t), e_i(t)} \int_{t_i^0}^{t_i^f} \left(\beta e_i^2(t) + \frac{1}{2}(u_i(t) - u_{ref}(t))^2\right) dt \quad (48)$$

subject to the vehicle dynamics (1), the CBF constraints (43) derived from (4), (5), (7), (6) and the CLF constraint (47). As already mentioned, we select $u_{ref}(t) = u_i^*(t)$ and, similarly, $v_{ref}(t) = v_i^*(t)$ in the CLF $V(\boldsymbol{x}_i(t)) = (v_i(t) - v_{ref}(t))^2$, but extend these in Section V-A.

With all constraints converted to CBF constraints in (48), we can solve this problem by discretizing $[t_i^0, t_i^f]$ into intervals $[t_i^0, t_i^0 + \Delta], \ldots, [t_i^0 + k\Delta, t_i^0 + (k+1)\Delta], \ldots$ of equal length Δ and solving (48) over each time interval. The decision variables $u_k = u_i(t_k)$ and $e_k = e_i(t_k)$ are assumed to be constant on each such time interval and can be easily obtained by solving a Quadratic Program (QP) problem:

$$\min_{u_k, e_k} \beta e_k^2 + \frac{\Delta}{2}(u_k - u_{ref}(t_i^0 + k\Delta))^2 \quad (49)$$

subject to the CBF constraints (43) and the CLF constraint (47), all evaluated at t_k, where all CBF and CLF constraints are linear in the decision variables u_k and e_k. By repeating this process until CAV i exits the CZ, the solution to (48) is obtained.

The computational cost in using OCBF is that of solving a Quadratic Program (QP) as shown in (49) at each time step. The cost of QP solutions is minimal and, in practice, it is less than 0.01 sec. By comparison, a complete solution of the

optimal control problem (10), may require one or two orders of magnitude more (about 0.3 to 30 seconds). Similarly, an MPC-based approach is also an order of magnitude slower (about 0.5 second). All the computation times are measured in MATLAB.

A. Reference Trajectory with Feedback

As already mentioned, in (48) we can select the simplest and most straightforward $u_{ref}(t) = u_i^*(t)$ along with $v_{ref}(t) = v_i^*(t)$ in the CLF $V(\boldsymbol{x}_i(t)) = (v_i(t) - v_{ref}(t))^2$. These simple reference trajectories work well in problems where the deviations $(u_i(t) - u_{ref}(t))$ are not exceedingly large, as observed, for instance, in optimal merging [15] and intersection control [16] problems. However, when the constraints become complex, especially when traffic in the roundabout becomes heavy, tracking these simple reference trajectories in an open-loop way often results in such large deviations from the unconstrained optimal solution (as illustrated in Section VI). Thus, a reference trajectory which includes feedback is introduced to solve this issue. In particular, we set

$$v_{\text{ref}}(t) = \frac{x^*(t)}{x(t)} v^*(t), \quad u_{\text{ref}}(t) = \frac{x^*(t)}{x(t)} u^*(t), \tag{50}$$

where $x(t)$ is the actual observed CAV position.

We also introduce another type of position-feedback to resolve the problem related to large deviations in t between the reference and actual trajectories, as illustrated through a specific numerical example in Fig. 7, further discussed in Section VI-B3. We calculate a reference time t_{ref} by solving the following equation at any t:

$$x^*(t_{\text{ref}}) = x(t) \tag{51}$$

where $x^*(\cdot)$ is the optimal unconstrained position of a given CAV in (26). Then, we choose the unconstrained optimal trajectory at t_{ref} as the reference $v_{\text{ref}}(t) = v^*(t_{\text{ref}})$ and $u_{\text{ref}}(t) = u^*(t_{\text{ref}})$ or

$$v_{\text{ref}}(t) = v^*((x^*)^{-1}(x(t))), \quad u_{\text{ref}}(t) = u^*((x^*)^{-1}(x(t))) \tag{52}$$

We will show how this approach can improve performance in Section VI-B3.

VI. Simulation Results

In this section, we use Vissim, a multi-model traffic flow simulation platform, as a baseline to evaluate traffic performance in roundabouts with human-driven vehicles and compare it to the performance obtained using our OCBF controller (for all CAVs). We use the model shown in Fig. 1 constructed in Vissim and use the same vehicle arrival patterns in the human-driven vehicle baseline and under the OCBF controller for consistent comparison purposes.

A. Virtual roundabout example

We first conduct a case study based on a virtual roundabout as shown in Fig. 1. The parameter settings are as follows: $L_a = 100m$, $L = 100m$, $\delta = 0m$, $\varphi = 1.8s$, $v_{\max} = 20m/s$, $v_{\min} = 0$, $u_{\max} = 5m/s^2$, $u_{\min} = -5m/s^2$.

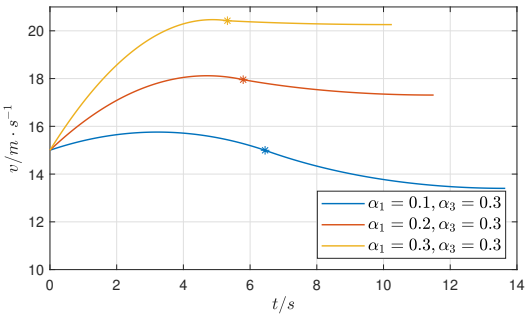

Fig. 2. Velocity trajectory under different travel time weights α_1. The asterisk shows the point when the CAV enters the circular part of the roundabout from the straight road segment.

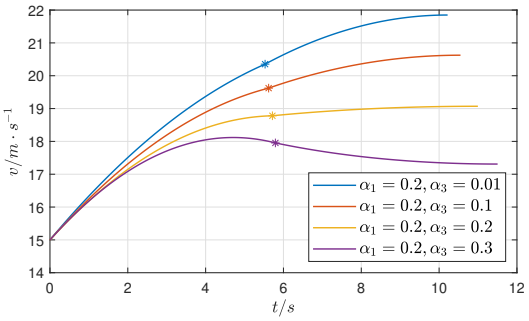

Fig. 3. Velocity trajectory under different comfort weights α_3. The asterisk shows the point when the CAV enters the circular part of the roundabout from the straight road segment.

This example considers a *symmetric* configuration in the sense that $L_a = L$. Different weights $\alpha_1, \alpha_2, \alpha_3$ directly influence the unconstrained optimal trajectory of a CAV. To explore this impact and determine a proper parameter setting for the weights, we start with the analysis of a single CAV that enters O_1 with initial speed $v_0 = 15m/s$ and exits from E_2 and plot the unconstrained optimal velocity trajectory under different weight settings in Figs. 2 and 3. In Fig. 2 the weight for travel time α_1 differs from the weight for comfort fixed at $\alpha_3 = 0.3$, while in Fig. 3 α_1 is fixed at 0.2 with changing α_3. Figure 2 shows that when comfort is taken into consideration with weight $\alpha_3 = 0.3$, the optimal control as the weight on time α_1 changes is for the CAV to go through the roundabout with a similar velocity trajectory but with higher speed. Figure 3 shows the influence of the comfort weight α_3. When α_3 decreases with α_1 fixed, the CAV adopts a higher speed in the circular part.

In what follows we will focus on the weight parameter settings: $\alpha_1 = 0.2, \alpha_2 = 0.5, \alpha_3 = 0.3$ to better illustrate the benefits of OCBF when the unconstrained velocity trajectory is within the speed limit. We will further discuss the benefits of a reference trajectory with feedback when this is not the case in Section VI-B3. We compare the OCBF controller with the human-driven vehicle Vissim baseline by simulating the same *symmetric* vehicle arrival pattern. The traffic in the three incoming roads is generated through Poisson processes and is *symmetric* in the sense that they all have the same traffic

rates. Two scenarios corresponding to a normal traffic rate of 400 CAVs/h and a high traffic rate of 600 CAVs/h are simulated. The former traffic rate allows vehicles to smoothly pass the roundabout with occasional wait or stop in Vissim, while the latter can sometimes form queues at the entry points before the merging points. The two traffic rates are selected based on observations of Vissim simulations so as to present scenarios with different road saturation (roughly 66.7% and 100% respectively). A total number of approximately 200 CAVs are simulated in both cases. In this example, the OCBF controller is applied with the SDF rule (see Section III-C) and the reference trajectory is generated *without* feedback. The results comparing the performance of OCBF to that of human-driven vehicles in Vissim are shown in Table III.

TABLE III
PERFORMANCE COMPARISON FOR A SYMMETRIC ROUNDABOUT UNDER SYMMETRIC TRAFFIC INPUT

Traffic rate	400 CAVs/h		600 CAVs/h	
Methods	OCBF	Vissim	OCBF	Vissim
Ave. time (s)	21.00	19.77	28.49	36.87
Ave. energy	17.67	34.78	32.73	57.35
Ave. comfort	58.36	74.10	47.98	60.96
Ave. obj. (energy)	175.20	200.32	218.37	296.56
Ave. fuel (mL)	19.64	13.39	19.92	14.59
Ave. obj. (fuel)	177.17	178.92	205.56	253.81

When the traffic rate is 400 CAVs/h, there is a 6% loss in the average travel time of CAVs using OCBF compared to that in Vissim due to the emphasis on energy and comfort which are improved by 49% and 21% respectively. The OCBF controller also shows a 12.5% improvement in the total objective over the human-driven performance in Vissim. On the other hand, when the traffic rate becomes 600 CAVs/h (which results in congestion), there is an improvement of 23% in the travel time (despite the low weight of $\alpha_1 = 0.2$ on travel time), 43% in the energy consumption, 20% in the comfort cost, and 26.5% in the total objective using OCBF relative to Vissim. This improvement in all the metrics is to be expected as the CAVs using the OCBF method never stop and wait for CAVs in other road segments to go through, which is the case in Vissim.

In Table III, we also include another performance metric that captures fuel consumption through a detailed model compared to the simple "energy" metric $\frac{1}{2}u^2$. The fuel consumption is measured using the model introduced in [33] using the set of parameters given in [34]:

$$f_V = f_{\text{cruise}} + f_{\text{accel}} \tag{53}$$

where $f_{\text{cruise}} = b_0 + b_1 v + b_2 v^2 + b_3 v^3$ represents the fuel consumption of cruising, $f_{\text{accel}} = u(c_0 + c_1 v + c_2 v^2)$ represents the fuel consumption of acceleration. The OCBF controller (which is not designed to explicitly minimize f_V) consumes about 40% more fuel than the car-following model used in Vissim; however, since we do not know the details of the Vissim fuel consumption model, the importance of this comparison should be discounted. Nonetheless, a higher fuel consumption under OCBF is justified due to the following two reasons: (i) a CAV consumes more fuel when cruising at a higher speed - which is selected by CAVs to improve travel times, (ii) the quadratic criterion $\frac{1}{2}u^2$ discourages large deceleration, whereas deceleration consumes no fuel according to [33]. On the other hand, leaving deceleration unpenalized slows traffic down and promotes backlog. Nevertheless, despite this difference, the total objective with fuel consumption included is still improved using OCBF as shown in Table III.

Finally, we note that if fuel consumption as measured through f_V above becomes an optimization objective, this can be accomplished using a numerical optimization approach which makes use of CBFs to still guarantee all constraints; this was shown in [15].

B. Real Roundabout

We consider next a real roundabout as shown in Fig. 4 located near Fresh Pond in Boston, MA, with the geometric parameters $L_1 = 186m, L_2 = 165m, L_3 = 196m, L_{a,1} = L_{a,2} = 53m, L_{a,3} = 63m$. This roundabout is asymmetric with a small circle and three long entries. The remaining settings are the same as in Section VI-A, i.e., $\delta = 0m$, $\varphi = 1.8s$, $v_{\max} = 20m/s$, $v_{\min} = 0$, $u_{\max} = 5m/s^2$, $u_{\min} = -5m/s^2$. We start with the same weight parameter settings: $\alpha_1 = 0.2, \alpha_2 = 0.5, \alpha_3 = 0.3$ and compare the performance of OCBF (with the SDF rule and no feedback) to the human-driven vehicle performance in Vissim under two different traffic rates 600 CAVs/h and 800 CAVs/h. The simulation results are shown in Table IV. Sample snapshots of the Vissim and MATLAB simluation respectively are shown in Fig. 5 and Fig. 6 at the same time instant.

TABLE IV
PERFORMANCE COMPARISON FOR AN ASYMMETRIC REAL ROUNDABOUT UNDER SYMMETRIC TRAFFIC INPUT

Traffic rate	600 CAVs/h		800 CAVs/h	
Methods	OCBF	Vissim	OCBF	Vissim
Ave. time (s)	18.97	27.44	22.28	39.13
Ave. energy	49.50	62.60	63.82	74.34
Ave. comfort	41.65	35.83	37.83	30.22
Ave. obj. (energy)	165.44	217.94	194.35	285.30
Ave. fuel	21.57	11.66	19.96	12.49
Ave. obj. (fuel)	137.52	167.00	150.48	223.45

As illustrated in Fig. 5, a backlog always forms in the Vissim simulation which requires vehicles to stop and queue before entering the circular road segment. The OCBF method, however, allows the CAVs to move faster and smoothly with *guaranteed* safety constraints without forming any backlogs (see Fig. 6). Although δ is set to 0, the CAVs using OCBF still keep an appropriate safety distance because of the φv_i term in (4); interestingly, these safety distances are actually larger than those observed between human-driven vehicles that use the car-following model in Vissim.

As shown in Table IV, CAVs using the OCBF controller improve performance on average by 31% in time, 21% in energy consumption and 24% in the total objective when the traffic rate is 600 CAVs/h, which is consistent with the results of the example in Section VI-A. An additional 8% improvement in the total objective is achieved under the high

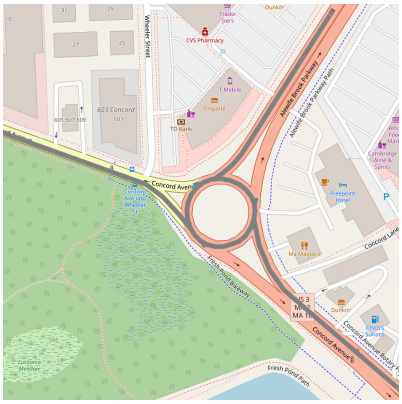

Fig. 4. An asymmetric roundabout near Fresh Pond in Boston, MA

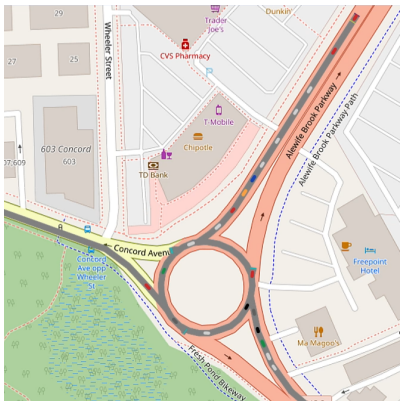

Fig. 5. Vissim simulation of human-driven behavior

Fig. 6. Matlab simulation of OCBF controller

traffic rate of 800 CAVs/h. Note that although the comfort cost is included in the total objective with weight 0.3, the OCBF controller still incurs a 16% higher comfort cost. This can be explained by the backlog formed by human-driven vehicles in Vissim shown in Fig. 5. As the queuing vehicles stop before entering and re-accelerate from zero speed in the circle, they result in a lower *average* velocity than those using the OCBF controller (thus, the actual comfort experience wihin the circular road segment is misrepresented by the average comfort data). The fuel consumption and the associated total objective using the model in [33], instead of the simple metric $\frac{1}{2}u^2$, are also included in Table IV showing similar results to those of Section VI-A.

In the following subsections, the settings of the OCBF controller are changed and simulated to explore the influence of weights, sequencing rules, feedback as well as asymmetric incoming traffic.

1) Time vs. comfort: In this case study, the travel time weight is fixed to $\alpha_1 = 0.2$ while the weight of comfort α_3 is changed from 0.3 to 0.01, representing almost no emphasis on comfort. The OCBF controller uses the SDF rule (see Section III-C) and tracks the reference trajectory with feedback. Simulation results under the traffic rate of 800 CAVs/h is recorded in Table V.

TABLE V
PERFORMANCE COMPARISON FOR AN ASYMMETRIC REAL ROUNDABOUT UNDER SYMMETRIC TRAFFIC INPUT

Methods	OCBF		Vissim	
Weight of comfort α_3	0.3	0.01	0.3	0.01
Ave. time (s)	22.65	21.84	39.13	
Ave. energy	64.61	61.95	74.34	
Ave. comfort	37.12	39.27	30.22	
Ave. obj. (energy)	196.63	131.47	285.30	198.49

As shown in Table V, the OCBF controller achieves better performance both when $\alpha_3 = 0.3$ and $\alpha_3 = 0.01$, with improvements of over 30% in the total objective. The average travel time as well as energy consumption decreases while the comfort cost increases when $\alpha_3 = 0.01$. This is reasonable as more emphasis is placed on energy consumption instead of comfort. As the comfort cost is a quadratic function of speed, a larger comfort cost indicates a higher velocity which results in shorter travel time.

2) Effect of Sequencing Rules: In this set of simulations, the effect of different sequencing rules is explored using both a symmetric roundabout (the virtual one) and an asymmetric roundabout (the real one). Simulation results on the performance of OCBF with FIFO and OCBF with the SDF sequencing policy are shown in Table VI.

TABLE VI
PERFORMANCE COMPARISON FOR DIFFERENT SEQUENCING RULES UNDER SYMMETRIC TRAFFIC INPUT

Roundabout geometry	Asymmetric		Symmetric	
Sequencing rule	FIFO	SDF	FIFO	SDF
Ave. time (s)	57.51	18.97	34.31	28.49
Ave. energy	141.37	49.50	39.61	32.73
Ave. comfort	14.27	41.65	43.66	47.98
Ave. obj. (energy)	436.14	165.44	250.44	218.37

When OCBF+FIFO is applied in a symmetric roundabout, it performs worse than OCBF+SDF in average travel time (20%), energy consumption (20%) as well as the total objective (14%). Comparing Table VI with Table III, it can be seen that the CAVs still benefit from the OCBF controller regardless of the sequencing policy selected. However, when OCBF+FIFO is applied to an asymmetric roundabout, the traffic becomes congested and the results become unstable even after simulating only 50 CAVs, indicating that FIFO works poorly in an asymmetric roundabout. For example, when a CAV enters segment l_4, it has to wait for another CAV that has entered l_2 just before it to drive more than 100 meters for safe merging. This is unreasonable and may also result in some extreme cases where the OCBF problem becomes infeasible. On the other hand, OCBF+SDF still achieves better and reliable performance in an asymmetric setting.

3) Reference Trajectory with Feedback: Here, the influence of feedback is studied. As mentioned in Section V-A, the reference trajectory without feedback may become unreliable due to the exponential terms that appear in (24) and (25) which result in large values when the time in the roundabout t is large. This is illustrated with the simulation results shown in Table VII for two different symmetric traffic rates 600

CAVs/h and 800 CAVs/h with the weight parameters set to $\alpha_1 = 0.2, \alpha_3 = 0.01$. When the traffic rate is 600 CAVs/h, using OCBF with feedback has a minimal effect on performance, contributing only a 4% improvement in the total objective. However, when the traffic rate increases to 800 CAVs/h, the roundabout becomes congested when CAVs are CAVs are controlled by OCBF without feedback, resulting in the explosive average travel time and energy consumption reflected in Table VII. This instability can be explained by the extended unconstrained optimal speed trajectory of a typical CAV plotted in Fig. 7.

TABLE VII
PERFORMANCE COMPARISON FOR AN ASYMMETRIC REAL ROUNDABOUT UNDER SYMMETRIC TRAFFIC INPUT

Traffic rate	600 CAVs/h		800 CAVs/h	
Feedback	No	Yes	No	Yes
Ave. time (s)	19.22	18.92	111.70	21.84
Ave. energy	52.97	49.64	99.82	61.95
Ave. comfort	42.87	43.61	15.26	39.27
Ave. obj. (energy)	114.26	109.99	453.46	131.47

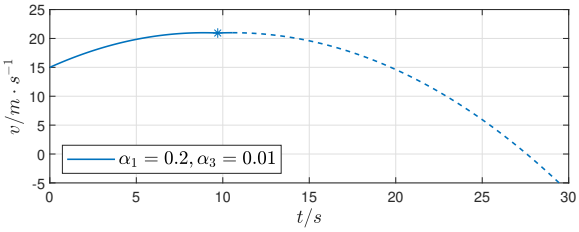

Fig. 7. Extended unconstrained optimal trajectory

In Fig. 7, the unconstrained optimal speed trajectory is shown as the solid blue line, where the terminal time t_f is marked with an asterisk. Note that t_f here corresponds to the unconstrained problem and is determined by (27), so in the actual constrained trajectory implemented through the OCBF controller the CAV is still in the CZ for times $t > t_f$. This "extended" speed trajectory is shown with the dashed line. When the traffic is heavy and results in considerable delay, the reference trajectory required by the OCBF controller is the one shown by the dashed line in Fig. 7. The reference speed will even drop to 0 after 27s in this example. Thus, the OCBF controller will track the inappropriate reference speed, which induces the CAV to stop and consequently block traffic. However, when a referenced trajectory with feedback (52) is used, the controller will map the current state of the CAV to the point on the solid curve in Fig. 7 and thus solve the issue related to selecting the proper time t on the reference trajectory.

4) Imbalanced Traffic: The purpose of this case study is to investigate the effect of traffic volume. A total number of approximately 200 CAVs is simulated under imbalanced incoming traffic (900 CAVs/h from O_1, 450 CAVs/h from O_2 and O_3). The simulation results of the performance under OCBF+SDF compared to that of the human-driven vehicles in Vissim under imbalanced incoming traffic are shown in Table VIII.

TABLE VIII
PERFORMANCE COMPARISON FOR AN ASYMMETRIC REAL ROUNDABOUT UNDER ASYMMETRIC TRAFFIC INPUT

Method	CAV Origin	Time	Energy	Comfort	Ave. Obj
OCBF	All	18.28	45.63	42.24	158.45
	O_1	19.38	44.01	42.14	162.27
	O_2	16.13	41.68	39.35	142.27
	O_3	18.62	53.22	45.70	169.48
Vissim	All	28.87	69.25	36.09	231.88
	O_1	33.88	76.03	34.67	263.03
	O_2	26.90	71.27	33.24	222.61
	O_3	21.43	53.89	42.06	182.36

Comparing Table VIII with Table IV, it is seen that imbalanced traffic causes longer travel times (∼2s) and higher energy consumption (∼7%), although the total traffic rates are the same. The imbalanced traffic results in an imbalanced performance of CAVs from different origins. The CAVs originating from O_1 with heavy traffic perform worse than those from O_2 and O_3 where traffic is lighter. However, when OCBF+SDF is applied to the system, the imbalanced traffic brings no performance loss and becomes more balanced compared to human-driven vehicle traffic. This result is interesting because the OCBF approach does not explicitly take into account the fact that traffic is *imbalanced*. An explanation of this phenomenon is that the SDF policy gives CAVs from O_1 a higher priority as they are more likely to be the closest ones to the MP, while OCBF allows the CAVs to go through the roundabout quickly without stopping; therefore, the CAVs from a heavy traffic flow are less likely to get congested.

VII. Conclusions and Future Work

We have presented a decentralized optimal control framework for controlling CAVs traveling through a circular roundabout to jointly minimize the travel time, the energy consumption, and the centrifugal discomfort while satisfying speed-dependent safety constraints, as well as velocity and acceleration constraints. An OCBF controller, combining an unconstrained optimal control solution with CBFs, is designed and implemented to track the desired (unconstrained) trajectory while guaranteeing that all safety constraints and vehicle limitations are satisfied. Significant improvements are shown in the simulation experiments which compare the performance of the OCBF controller to a baseline of human-driven vehicles. Future research includes extending the OCBF controller to multiple-lane roundabout configurations and systematically studying the effect of the passing order. As for the multi-lane case (including the all-direction lane setting in [35]), we expect that our analysis will follow the same natural extensions we have already applied for merging [25] and for signal-free intersections [26]. In addition, we are currently exploring how this framework can be adapted to mixed traffic, i.e., how CAVs can effectively interact with human driven vehicles and provide system-wide performance improvements.

Finally, Some technical issues regarding CBFs are still under study, including the fact that CBFs may be conservative in guaranteeing constraints at the expense of better overall performance.

APPENDIX
TRACKING THE REFERENCE TRAJECTORY IN TWO DIMENSIONS

In this Appendix, we introduce an auxiliary method to deal with the lateral offset while tracking the trajectory given by our OCBF controller. Our OCBF controller focuses on generating a reference trajectory with longitudinal safety guarantees in real time. The lateral error can be dealt with using a Model Predictive Control (MPC) tracking approach.

A. Vehicle Dynamics

We use the same vehicle dynamics as in our previous work [29]. Ego dynamics are defined in a 2-dimensional coordinate system with respect to a reference trajectory, where the x coordinate lies along the reference trajectory and the y coordinate refers to the lateral offset:

$$\underbrace{\begin{bmatrix}\dot{s}\\ \dot{d}\\ \dot{\mu}\\ \dot{v}\\ \dot{a}\\ \dot{\delta}\\ \dot{\omega}\end{bmatrix}}_{\dot{\boldsymbol{x}}} = \underbrace{\begin{bmatrix}\frac{v\cos(\mu+\beta)}{1-d\kappa}\\ v\sin(\mu+\beta)\\ \frac{v}{l_r}\sin\beta-\kappa\frac{v\cos(\mu+\beta)}{1-d\kappa}\\ a\\ 0\\ \omega\\ 0\end{bmatrix}}_{f(\boldsymbol{x})} + \underbrace{\begin{bmatrix}0&0\\0&0\\0&0\\0&0\\1&0\\0&0\\0&1\end{bmatrix}}_{g(\boldsymbol{x})}\underbrace{\begin{bmatrix}u_{jerk}\\ u_{steer}\end{bmatrix}}_{\boldsymbol{u}} \tag{54}$$

where $s \in \mathbb{R}$ is the along-trajectory distance and $d \in \mathbb{R}$ is the lateral offset; μ is the vehicle local heading error; v, a denote the vehicle linear speed and acceleration; δ, ω denote the steering angle and steering rate; u_{jerk} and u_{steer} denote the two control inputs for jerk and steering acceleration; κ is the curvature of the reference trajectory at the projection point $(s, 0)$; $\beta = \arctan\left(\frac{l_r}{l_r+l_f}\tan\delta\right)$ where l_f (l_r) is the length of the vehicle from head (tail) to the CoG.

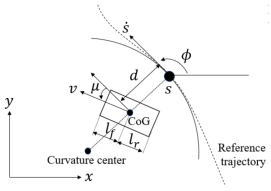

Fig. 8. Coordinates of ego vehicle w.r.t reference trajectory

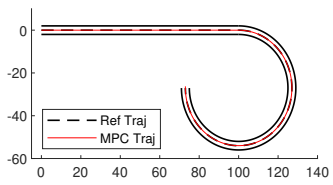

Fig. 9. Tracking performance of MPC

B. MPC controller design

To track the reference trajectory under the detailed vehicle dynamics shown in Sec. A, we adopt a receding horizon (MPC) approach that solves the following optimization problem with receding horizon H at each time $t \geq 0$:

$$(\boldsymbol{u}_{mpc}, \boldsymbol{x}_{mpc}) = \arg\min_{\boldsymbol{u}(0:H-1),\boldsymbol{x}(1:H)} \sum_{i=1}^{H} C(\boldsymbol{x}(i)) + \sum_{i=0}^{H-1} J(\boldsymbol{u}(i)) \tag{55}$$

where $C(\boldsymbol{x}(i))$ describes the tracking error with respect to the reference trajectory, $J(\boldsymbol{u}(i))$ is the penalty term for jerk and steering acceleration. For this specific problem, the two functions are defined as follows:

$$C(\boldsymbol{x}) = w_1(s-s_{ref})^2 + w_2(d-d_{ref}^2) + w_3(v-v_{ref})^2 \tag{56}$$

$$J(\boldsymbol{u}) = u_{jerk}^2 + u_{steering}^2 \tag{57}$$

For the prediction part, we use the following predictive model derived from (54) using the Adomian Decomposition Method (ADM):

$$\begin{bmatrix}s(k+1)\\ d(k+1)\\ \mu(k+1)\\ v(k+1)\\ a(k+1)\\ \delta(k+1)\\ \omega(k+1)\end{bmatrix} = \begin{bmatrix}s(k)+\frac{v(k)\cos(\mu(k)+\beta(k))}{1-d(k)\kappa(k)}\Delta T\\ d(k)+v(k)\sin(\mu(k)+\beta(k))\Delta T\\ \mu(k)+(\frac{v(k)}{l_r}\sin\beta(k)-\kappa(k)\frac{v(k)\cos(\mu(k)+\beta(k))}{1-d(k)\kappa(k))\Delta T}\\ v(k)+a(k)\Delta T+\frac{1}{2}u_{jerk}\Delta T^2\\ a(k)+u_{jerk}\Delta T\\ \delta(k)+\omega\Delta T+\frac{1}{2}u_{steer}\Delta T^2\\ \omega(k)+u_{steer}\Delta T\end{bmatrix} \tag{58}$$

C. Simulation Results

In this simulation example, we build a scenario consisting of a roundabout which connects a 3/4 circle with radius $r = 27m$ to a 100m length straight road segment. We use the MPC approach above to track the reference trajectory given by our OCBF controller presented in the paper. The first simulation is conducted without adding noise. The tracking performance of the MPC controller is shown in Fig. 9, where we can see the MPC trajectory precisely follows the center line of the road (also the reference trajectory).

The tracking error of the velocity v is shown in Fig. 10. While avoiding the lateral offset, the controller can also track the reference velocity as well as position accurately at the same time. This indicates that by using a reference trajectory tracking method like MPC, we can deal with the lateral offset while tracking our trajectory given by the OCBF controller without much effort.

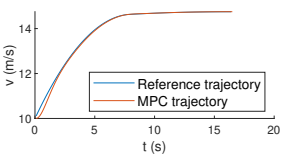

Fig. 10. Tracking error of v

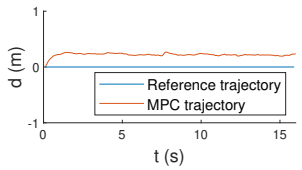

Fig. 11. Tracking error of d with *biased* noise

We further illustrate the effectiveness of the controller by adding noise to the vehicle dynamics. Uniform noise ranging over $[0, 1]$(m/s) is added both to the along-trajectory velocity $\dot{s}$ and the lateral offset velocity $\dot{\mu}$ which can represent model inaccuracies as well as some vehicle malfunction like imbalanced tire pressure which may result in a biased error. The tracking performance of d with noise added is shown in Fig. 11. Even when the biased noise is added, the vehicle can still track the reference trajectory well. The lateral offset error increases to around 20cm due to the large biased noise in $\dot{d}$,

but is still quite small. Furthermore, it always keeps its error level within this acceptable range and never diverges.

These simulation results support the argument that by using an auxiliary method like MPC, we are able to deal with lateral offset while tracking the trajectory given by our OCBF controller. Lastly, we note that the OCBF controller also has the ability to deal with the lateral offset by directly deriving CBFs from the vehicle dynamics (54).

REFERENCES

[1] J. Rios-Torres and A. A. Malikopoulos, "A survey on the coordination of connected and automated vehicles at intersections and merging at highway on-ramps," *IEEE Transactions on Intelligent Transportation Systems*, vol. 18, no. 5, pp. 1066–1077, 2016.

[2] L. Chen and C. Englund, "Cooperative intersection management: A survey," *IEEE Transactions on Intelligent Transportation Systems*, vol. 17, no. 2, pp. 570–586, 2015.

[3] M. Tideman, M. C. van der Voort, B. van Arem, and F. Tillema, "A review of lateral driver support systems," in *2007 IEEE Intelligent Transportation Systems Conference*, pp. 992–999, IEEE, 2007.

[4] L. Li, D. Wen, and D. Yao, "A survey of traffic control with vehicular communications," *IEEE Transactions on Intelligent Transportation Systems*, vol. 15, no. 1, pp. 425–432, 2013.

[5] H. Xu, S. Feng, Y. Zhang, and L. Li, "A grouping-based cooperative driving strategy for cavs merging problems," *IEEE Transactions on Vehicular Technology*, vol. 68, no. 6, pp. 6125–6136, 2019.

[6] H. Xu, Y. Zhang, C. G. Cassandras, L. Li, and S. Feng, "A bi-level cooperative driving strategy allowing lane changes," *Transportation research part C: emerging technologies*, vol. 120, p. 102773, 2020.

[7] V. Milanés, J. Godoy, J. Villagrá, and J. Pérez, "Automated on-ramp merging system for congested traffic situations," *IEEE Transactions on Intelligent Transportation Systems*, vol. 12, no. 2, pp. 500–508, 2010.

[8] J. Rios-Torres, A. Malikopoulos, and P. Pisu, "Online optimal control of connected vehicles for efficient traffic flow at merging roads," in *2015 IEEE 18th international conference on intelligent transportation systems*, pp. 2432–2437, IEEE, 2015.

[9] Y. Bichiou and H. A. Rakha, "Developing an optimal intersection control system for automated connected vehicles," *IEEE Transactions on Intelligent Transportation Systems*, vol. 20, no. 5, pp. 1908–1916, 2018.

[10] R. Hult, G. R. Campos, E. Steinmetz, L. Hammarstrand, P. Falcone, and H. Wymeersch, "Coordination of cooperative autonomous vehicles: Toward safer and more efficient road transportation," *IEEE Signal Processing Magazine*, vol. 33, no. 6, pp. 74–84, 2016.

[11] W. Cao, M. Mukai, T. Kawabe, H. Nishira, and N. Fujiki, "Cooperative vehicle path generation during merging using model predictive control with real-time optimization," *Control Engineering Practice*, vol. 34, pp. 98–105, 2015.

[12] M. Mukai, H. Natori, and M. Fujita, "Model predictive control with a mixed integer programming for merging path generation on motor way," in *2017 IEEE Conference on Control Technology and Applications (CCTA)*, pp. 2214–2219, IEEE, 2017.

[13] M. H. B. M. Nor and T. Namerikawa, "Merging of connected and automated vehicles at roundabout using model predictive control," in *2018 57th Annual Conference of the Society of Instrument and Control Engineers of Japan (SICE)*, pp. 272–277, IEEE, 2018.

[14] W. Xiao and C. Belta, "High order control barrier functions," in *IEEE Transactions on Automatic Control, doi:10.1109/TAC.2021.3105491*, 2021.

[15] W. Xiao, C. G. Cassandras, and C. A. Belta, "Bridging the gap between optimal trajectory planning and safety-critical control with applications to autonomous vehicles," *Automatica*, vol. 129, p. 109592, 2021.

[16] Y. Zhang and C. G. Cassandras, "Decentralized optimal control of connected automated vehicles at signal-free intersections including comfort-constrained turns and safety guarantees," *Automatica*, vol. 109, p. 108563, 2019.

[17] W. Xiao and C. G. Cassandras, "Decentralized optimal merging control for connected and automated vehicles with safety constraint guarantees," *Automatica*, vol. 123, p. 109333, 2021.

[18] A. Flannery and T. Datta, "Operational performance measures of american roundabouts," *Transportation research record*, vol. 1572, no. 1, pp. 68–75, 1997.

[19] M. Martin-Gasulla, A. García, and A. T. Moreno, "Benefits of metering signals at roundabouts with unbalanced flow: Patterns in spain," *Transportation Research Record*, vol. 2585, no. 1, pp. 20–28, 2016.

[20] X. Yang, X. Li, and K. Xue, "A new traffic-signal control for modern roundabouts: method and application," *IEEE Transactions on Intelligent Transportation Systems*, vol. 5, no. 4, pp. 282–287, 2004.

[21] H. Xu, K. Zhang, and D. Zhang, "Multi-level traffic control at large four-leg roundabouts," *Journal of Advanced Transportation*, vol. 50, no. 6, pp. 988–1007, 2016.

[22] L. Zhao, A. Malikopoulos, and J. Rios-Torres, "Optimal control of connected and automated vehicles at roundabouts: An investigation in a mixed-traffic environment," *IFAC-PapersOnLine*, vol. 51, no. 9, pp. 73–78, 2018.

[23] B. Chalaki, L. E. Beaver, and A. A. Malikopoulos, "Experimental validation of a real-time optimal controller for coordination of cavs in a multi-lane roundabout," in *2020 IEEE Intelligent Vehicles Symposium (IV)*, pp. 775–780, IEEE, 2020.

[24] K. Xu, C. G. Cassandras, and W. Xiao, "Decentralized time and energy-optimal control of connected and automated vehicles in a roundabout," in *2021 IEEE International Intelligent Transportation Systems Conference (ITSC)*, pp. 681–686, 2021.

[25] W. Xiao, C. G. Cassandras, and C. Belta, "Decentralized optimal control in multi-lane merging for connected and automated vehicles," in *2020 IEEE 23rd International Conference on Intelligent Transportation Systems (ITSC)*, pp. 1–6, 2020.

[26] H. Xu, W. Xiao, C. G. Cassandras, Y. Zhang, and L. Li, "A general framework for decentralized safe optimal control of connected and automated vehicles in multi-lane signal-free intersections," *IEEE Transactions on Intelligent Transportation Systems*, pp. 1–15, 2022.

[27] H. Xu, C. G. Cassandras, L. Li, and Y. Zhang, "Comparison of cooperative driving strategies for cavs at signal-free intersections," *IEEE Transactions on Intelligent Transportation Systems (to apperar)*, pp. 1–14, 2021.

[28] Y. Zhang and C. G. Cassandras, "A decentralized optimal control framework for connected automated vehicles at urban intersections with dynamic resequencing," in *2018 IEEE Conference on Decision and Control (CDC)*, pp. 217–222, IEEE, 2018.

[29] W. Xiao, N. Mehdipour, A. Collin, A. Y. Bin-Nun, E. Frazzoli, R. D. Tebbens, and C. Belta, "Rule-based evaluation and optimal control for autonomous driving," 2021.

[30] K. Vogel, "A comparison of headway and time to collision as safety indicators," *Accident analysis & prevention*, vol. 35, no. 3, pp. 427–433, 2003.

[31] J. Pinnow, M. Masoud, M. Elhenawy, and S. Glaser, "A review of naturalistic driving study surrogates and surrogate indicator viability within the context of different road geometries," *Accident Analysis & Prevention*, vol. 157, p. 106185, 2021.

[32] W. Xiao and C. G. Cassandras, "Decentralized optimal merging control for connected and automated vehicles on curved roads," in *2021 IEEE Conference on Decision and Control (CDC)*, pp. 2677–2682, IEEE, 2021.

[33] M. A. S. Kamal, M. Mukai, J. Murata, and T. Kawabe, "Ecological vehicle control on roads with up-down slopes," *IEEE Transactions on Intelligent Transportation Systems*, vol. 12, no. 3, pp. 783–794, 2011.

[34] M. A. S. Kamal, M. Mukai, J. Murata, and T. Kawabe, "Model predictive control of vehicles on urban roads for improved fuel economy," *IEEE Transactions on Control Systems Technology*, vol. 21, no. 3, pp. 831–841, 2013.

[35] W. Wu, Y. Liu, W. Liu, F. Zhang, V. Dixit, and S. T. Waller, "Autonomous intersection management for connected and automated vehicles: A lane-based method," *IEEE Transactions on Intelligent Transportation Systems*, pp. 1–16, 2021.

Kaiyuan Xu received his B.S. and M.S. degree from Tsinghua University, China in 2016 and 2019 respectively. He is currently pursuing his PhD degree in Systems Engineering at Boston University, Brookline, MA, USA.

His research interests include optimization-based control theory and methodology for large-scale complex systems through data-driven, statistical, and computational analysis with applications to transportation systems, robotics systems, cyber physical systems and biological systems.

Christos G. Cassandras (F'96) received a BS degree (Engineering and Applied Science) from Yale University, New Haven, CT, USA, a M.S.E.E. degree from Stanford University, Stanford, CA, USA, and S.B. and Ph.D. degrees (Applied Mathematics) from Harvard University, Cambridge, MA, USA. In 1982–1984, he was with ITP Boston, Inc. In 1984–1996, he was a Faculty Member with the Department of Electrical and Computer Engineering, University of Massachusetts/Amherst. He is currently a Distinguished Professor of Engineering with Boston University, Brookline, MA, USA, the Head of the Division of Systems Engineering, and Professor of Electrical and Computer Engineering. He has authored or coauthored six books, and 500 refereed papers in the areas of discrete event and hybrid systems, cooperative control, stochastic optimization, and computer simulation, with applications to computer and sensor networks, manufacturing systems, and transportation systems.

Dr. Cassandras serves on several journal Editorial Boards and was the Editor-in-Chief of the IEEE TRANSACTIONS ON AUTOMATIC CONTROL (1998-2009). He was the 2012 President of the IEEE Control Systems Society (CSS). He has been a plenary/keynote speaker at numerous international conferences and has also been an IEEE Distinguished Lecturer. He is the recipient of several awards, including the 2011 IEEE Control Systems Technology Award, the Distinguished Member Award of the IEEE Control Systems Society (2006), the 1999 Harold Chestnut Prize (IFAC Best Control Engineering Textbook) among others. He is a Member of Phi Beta Kappa and Tau Beta Pi. He is also a Fellow of the IFAC.

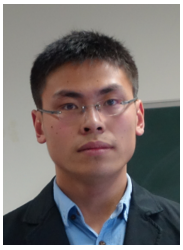

Wei Xiao (S'19) is currently a postdoctoral associate at Massachusetts Institute of Technology. He received a B.Sc. degree from the University of Science and Technology Beijing, China in 2013, a M.Sc. degree from the Chinese Academy of Sciences (Institute of Automation), China in 2016, and a Ph.D. degree from the Boston University, Brookline, MA, USA in 2021. His research interests include control theory and machine learning, with particular emphasis on robotics and traffic control. He received an Outstanding Student Paper Award at the 2020 IEEE Conference on Decision and Control.